



Dual disorder-driven magnetic dynamics in GdCu₂ superantiferromagnetic nanoparticles

Elizabeth M Jefremovas · Peter Svedlindh · Luis Fernández Barquín

Received: 21 April 2022 / Accepted: 8 September 2022 / Published online: 21 September 2022
© The Author(s) 2022

Abstract The spin dynamics in magnetically disordered GdCu₂ nanoparticles, varying the nanoparticle size in the range 53 to 7 nm, has been scrutinized. Dynamic χ_{AC} susceptibility measurements have revealed the existence of dissipation at $T_g = 18$ K, which is associated to the spin freezing transition, for all the ensembles. Besides, the superantiferromagnetic ensembles ($\langle D \rangle \geq 24$ nm) also showcase a dissipation contribution close to the vicinity of the Néel

transition, $T_N = 40.2$ K. This dissipation, which takes the form of two humps located at $T_{d1} = 33.5(5)$ K and $T_{d2} = 40.0(5)$ K, is associated to uncompensated antiferromagnetic moments. Time-dependent phenomena (ageing and memory effects) are only evidenced below the spin freezing transition, evidencing that solely this low-temperature disordered phase is driven by the frustration of RKKY exchange interactions. Consequently, GdCu₂ nanoparticles display a dual disorder-driven magnetic dynamics, which are the one ascribed to the magnetically frustrated moments located at the nanoparticle surface; and that of uncompensated antiferromagnetic moments located within the nanoparticle core.

Highlights

Two magnetically disordered phases observed in GdCu₂ magnetic nanoparticles. Non-conventional time dependent AC susceptibility ageing and memory effects phenomena used to probe the disorder spin dynamics. Non-frustrated high-temperature magnetically disordered phase associated to uncompensated AF grain boundaries. Spin glass low-temperature phase driven by surface (53–24-nm-sized nanoparticles) and whole nanoparticle (13- and 9-nm-sized) magnetically frustrated moments. The joint analyses of time-dependent AC susceptibility plus specific heat measurements allow to depict that superantiferromagnetic GdCu₂ nanoparticles (53- to 24-nm-sized) evidence two different magnetically disordered phases, while for the super spin glass ones (13 and 9 nm), only the frustrated low-temperature disordered phase remains.

Keywords Magnetic nanoparticles · Antiferromagnetism · Frustrated magnetism · Spin dynamics

Introduction

Over the last years, the spin dynamics of magnetic ensembles, including mesoscopic ones, has received increasing interest. Their technological transfer, specially focused on the spintronics fields, has been the driving force motivating the experimental and theoretical efforts to clearly understand how the size reduction to the nanoscale affects the magnetic properties (Golosovsky et al. 2021; Baczewski et al. 1989; Jefremovas et al. 2020a, 2021; Zhao et al. 2019).

E. M. Jefremovas (✉) · L. F. Barquín
Department CITIMAC, Facultad de Ciencias, Universidad de Cantabria, 39005 Santander, Spain
e-mail: martinjel@unican.es

P. Svedlindh
Department of Materials Science and Engineering,
Uppsala University, Box 35, SE-751 03 Uppsala, Sweden

Within this context, antiferromagnetic (AF) nanoensembles have attracted a lot of interest in recent years, owing to their inherent assets (e.g., anomalous Hall effect, anisotropic magnetoresistance, long-distance spin-wave propagation (Marti et al. 2014; Nakatsuji et al. 2015; Lebrun et al. 2018)). It is also worth mentioning that the complex magnetic arrangements found in AF materials makes them potential candidates for hosting exotic spin textures, as it is the case of skyrmions (Zhang et al. 2016; Fukami et al. 2020; Jungwirth et al. 2016; Jungfleisch et al. 2018; Everschor-Sitte et al. 2018; Park and Kim 2021). It is within this context that the determination of the spin dynamics governed by disordered and frustrated magnetic interactions is key, since the magnetic frustration arising from RKKY interactions have shown to be helpful in stabilizing these topologically protected spin textures (Greedan 2006; Zvyagin 2013; Tokura and Kanazawa 2020; von Malottki et al. 2017; Yuan et al. 2017).

Among the Rare-Earth binary alloys, the GdCu₂ bulk alloy displays an AF structure (Rotter et al. 2000b), which is maintained down to 24-nm-sized magnetic nanoparticles (MNPs), all along with the onset of a frustrated Spin Glass (SG) phase at low temperature (Jefremovas et al. 2020b). Among the R elements, Gd³⁺-ions display a half-filled 4f shell, implying absence of spin-orbit interaction. This leads Gd³⁺ to be in an *intermediate* situation between that of 3d and 4f magnetism. The S-state of Gd³⁺ also implies the lack of magnetocrystalline anisotropy for this ion, which certainly eases theoretical modeling and calculations. Thus, Gd³⁺ has been more and more included in compounds to understand their magnetism at the basis, as it has been the case of the recent study reported by P.G. Welch et al., where the spin dynamics of the Heisenberg pyrochlore antiferromagnet Gd₂Pt₂O was unraveled (Welch et al. 2022). Furthermore, Gd³⁺ displays, along with Tb³⁺, one of the greatest effective magnetic moments ($\mu_{eff} = 7.94\mu_B$), which constitutes another asset to determine subtle modifications in the interaction among the magnetic moments. This has been useful, for instance, to reveal the existence of two-length scales reported for nanocrystalline Gd (Döbrich et al. 2009), or, more recently, to reveal how the RKKY magnetic interactions were altered by the size reduction (Jefremovas et al. 2020b). In this latter work, Jefremovas et al. have determined 24 nm to be the limit size for

the bulk AF state to survive within the nanoparticle core, together with a surface SG phase, building the so-called *superantiferromagnetic (SAF)* state. The RKKY interactions of smaller nanoparticles are unable to establish a collective AF ordered state, and a Super Spin Glass (SSG) arrangement is settled instead. This lead GdCu₂ to display a particular magnetic order/disorder configuration depending upon the nanoparticle size. Indeed, a detailed study of the underlying spin dynamics is key to understand the modifications of the RKKY exchange interactions at the nanoscale.

Hence, in the present work, we carried out dynamic χ_{AC} susceptibility measurements, both in the temperature and frequency domains (T, f), and in the time domain (t), to unravel the nature behind the magnetic order/disorder phases found in GdCu₂ MNPs. Complementary, specific heat c_p measurements were analyzed to better determine the nature of the magnetic transitions. The present characterization is not so commonly found in the literature, and supplements the static picture of the magnetic properties of GdCu₂ MNPs reported in Jefremovas et al. (2020b).

Experimental details

Polycrystalline GdCu₂ pellets have been obtained in an arc furnace (MAM-1, Johanna Otto GmbH) under an Ar atmosphere (99.99%). The resulting pellet was crushed, sealed-off under Ar pressure (99.99%) to avoid the oxidation, and grinded for times ranging between 0.5 and 5 h in a high-energy planetary ball mill (Retsch PM 400/2). By doing so, we produced 6 different ensembles of MNPs, with average crystal sizes of 40, 32, 25, 18, 10 and 7 nm (Jefremovas et al. 2020b). A correspondence between the average crystal size and the mean nanoparticle size can be made taking into account a factor 4/3 (Guinier 1994). Therefore, the corresponding mean nanoparticle sizes are 53(5), 43(5), 33(5), 24(2), 13(1) and 9(1) nm.

The magnetic characterisation was performed by means of dynamic $\chi_{AC}(t, f, T)$ (*time, frequency and temperature, respectively*) measurements. These were carried out in two QD-MPMS (SQUID) magnetometers, one of which is located at the Uppsala University (Sweden), and the second one, at the Universidad de Cantabria (Spain). The ensembles of MNPs were measured in different temperature

ranges between $T = 5\text{--}300$ K. Oscillating fields $\mu_0 h = 0.1$ and 0.313 mT, and frequencies ranging from 0.17 Hz to 2 Hz were employed. To probe memory effects and ageing phenomena, several protocols can be found in the literature (Nordblad and Svedlindh 1998; Jönsson et al. 2000; Jonason et al. 1998; Joshi et al. 2020; Svedlindh et al. 1992). Here, we have probed both time-dependent phenomena by tracing the out-of-phase χ'' component of the dynamic χ_{AC} susceptibility, as it allows to detect in more detail the subtleties concerning the spin dynamics (Nordblad and Svedlindh 1998; Svedlindh et al. 1992; Jefremovas et al. 2022). Shortly, memory effects have been probed from the difference between the out-of-phase χ'' component measured (i) during cooling ($\chi''_{cooling}$), and (ii) upon warming ($\chi''_{warming}$). There is a difference between the measuring protocol used while cooling and warming. This way, during the cooling, a stop is made at $T_{ag} = 15$ and 30 K for $t > 10^3$ s. During this time, the system gets aged, and a particular spin disorder configuration (domain) can be settled. Then, the warming curve is measured without making any stop. The memory effect is then evidenced by the occurrence of a drop in $\chi''_{warming} - \chi''_{cooling}$ at temperatures slightly below T_g . Coming to the ageing phenomena, these can be easily detected by the inspection of the χ'' vs. t dependency. Moreover, the robustness of the SG-like frustrated interactions has been further investigated by applying a temperature cycling protocol. This consists of measuring the χ'' vs. t dependency at a certain temperature T_{ag} within the SG phase (in our case, $T_{ag} \sim 0.8T_g$) for a sufficiently long period of time ($t \sim 10^3$ s). After the waiting time, the temperature is raised to $T_{ag} + \Delta T$. In the case of the present work, ΔT was selected such that $T_{ag} + \Delta T$ was $0.85T_g$ and $1.1T_g$. Then, the temperature is lowered back to T_{ag} , and $\chi''(t)$ is measured again for $t \sim 10^4\text{--}10^5$ s. This cycling protocols mimics the one reported in ?svedlindh1992time,ageing_Eli ()).

Finally, heat capacity (c_p) measurements were performed using a QD-PPMS instrument (Universidad de Cantabria) in the temperature range $T = 2\text{--}300$ K. The measurements were collected in the absence of magnetic field. Measurements were performed following the relaxation method (Bachmann et al. 1972), and the data analyses follows the

surface-core separation already detailed in Jefremovas et al. (2021, 2022).

Results and discussion

Dynamic magnetic susceptibility vs. temperature

Figure 1a and b showcase the $\chi_{AC}(T)$ components (in-phase χ' and out-of-phase χ'' , respectively) measured at the frequency of $f = 0.17$ Hz for the 6 ensembles of MNPs. There, the occurrence of a cusp in both in-phase (Fig. 1a) and out-of-phase components (Fig. 1b) is clearly noticeable in the low-temperature region ($T < 25$ K). This has been interpreted as the onset of a SG-like phase, whose freezing dynamics has been characterized in great detail in Jefremovas et al. (2020b). Therefore, from herein, we will focus on the high temperature region, i.e., the one close to the Néel transition.

Therefore, in Fig. 1a, a peak associated with the AF transition is found at $T_N = 40.2$ K for MNPs larger than 24 nm, being absent for the smallest ones (13 and 9 nm). The temperature value of this peak does not evidence a size-dependence, as expected (Coeys 2010). Paying attention now to the out-of-phase component displayed in Fig. 1b, additionally to the onset of a low-temperature peak ($T_g \approx 18$ K), linked to the SG phase, a dissipation contribution is clearly detectable in the temperature range between 30 and 40 K, but only for the case of $\langle D \rangle \geq 24$ nm MNPs. More precisely, this dissipation takes the form of two humps, located at $T_{d1} = 33.5(5)$ K and $T_{d2} = 40.0(5)$ K for all these superantiferromagnetic (SAF) MNPs. The peaks broaden and reduce in magnitude with the size reduction, being completely wiped out when the limit size for AF order to remain is overcome (i.e., below 24 nm). The observation of dissipation connected to AF order is totally unexpected, as these should not exhibit, in principle, any contribution to the out-of-phase component (Coeys 2010). There is, however, one scenario where dissipation can be expected for AF MNPs, and it is found within the context of uncompensated magnetic moments associated to antiferromagnetic domains. This interpretation follows the same ideas previously proposed for NiO AF grain boundaries (Takano et al. 1997), and it is congruent with the static $M_{DC}(H)$ characterization described in Jefremovas et al. (2020b), where the

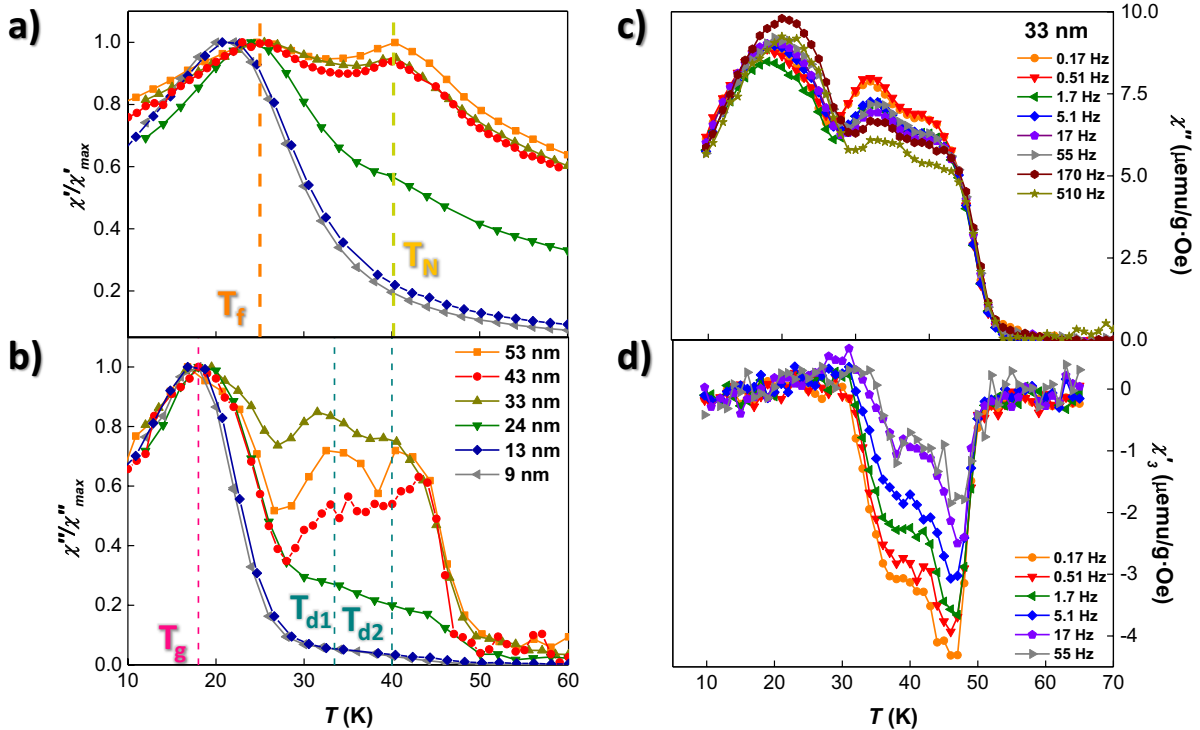


Fig. 1 **a)** **(b)** In-phase (out-of-phase) components, measured at $f = 0.17$ Hz and $h = 0.131$ mT, normalized by the in-phase (out-of-phase) value attained at the freezing (glass) transition. It is worth noting in **(b)** the presence of $T_{d1} \approx 33.5$ K and $T_{d2} \approx 40$ K peaks, additionally to the one of $T_g \approx 18$ K ascribed

evolution of the coercive field H_C with MNP size $\langle D \rangle$ reached a maximum for 24-nm-sized MNPs. A simple estimation based on the AF unit cell, which comprises 3 crystallographic-ones along b direction (Rotter et al. 2000a), leads to an AF correlation length of $3b \sim 2.1$ nm. Hence, the 24-nm-sized MNPs, for which a core size of $\langle D \rangle \sim 20$ nm can be estimated (Jefremovas et al. 2021, 2022; Rojas et al. 2007), are large enough to host up to 11 complete AF unit cells and the AF grain boundaries within. The fact that this dissipation takes the form of two well-defined and separated cusps is in further agreement with the AF structure of GdCu_2 .

According to neutron diffraction and muon spectroscopy resonance analyses (Rotter et al. 2000a; Gygax et al. 2002; Rotter et al. 2000b), GdCu_2 arranges into a commensurate AF structure carrying non-collinear cycloidal propagation. There are two different domains possible, one with a left-handed and another with a right-handed cycloid. Each of

to the freezing transition. **c)** depicts evolution of the χ'' vs. T measured at f between 0.17 and 510 Hz for the 33-nm-sized SAF MNPs. **d)** displays the non-linear χ'_3 component measured up to 55 Hz for the SAF 33-nm-sized MNPs. Note that, in **c)** and **d)**, the susceptibility units are $\mu \text{emu/gOe}$

these two domains should carry frequency-dependent dissipation, a fact that can be observed in Fig. 1c for the 33-nm-sized MNPs, as there is a progressive decrease of the χ'' component at T_{d1} and T_{d2} with increasing f . Furthermore, the trace of a high-temperature double-peak signature is also traced by the non-linear χ'_3 response, included in Fig. 1d. The lack of these two peaks also in the non-linear response corresponding to the SSG MNPs (13- and 9-nm-sized) necessarily connects this high-temperature dissipation to the AF structure.

Time-dependent phenomena: memory effects and ageing

Ageing and memory effect phenomena are intimately connected to the out-of-equilibrium dynamics of non-ergodic systems (SGs), thus proving the existence of highly correlated RKKY-frustrated spins (Svedlindh et al. 1992; Nordblad and Svedlindh 1998; Jonason

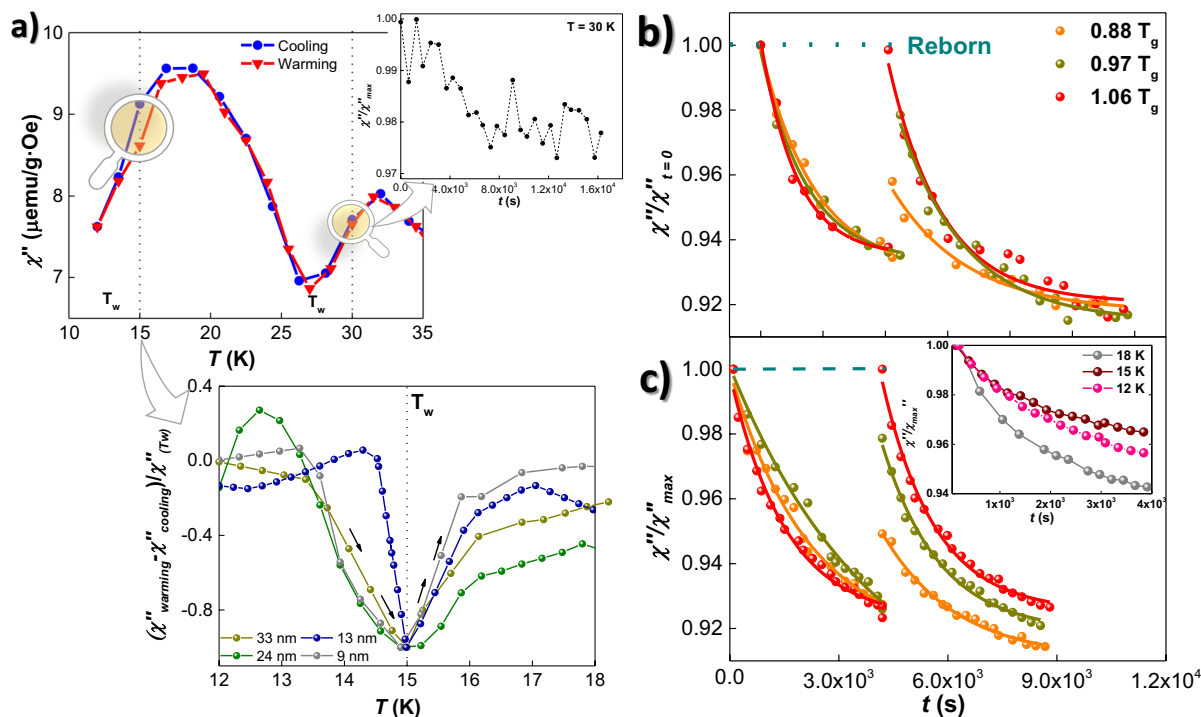


Fig. 2 a) Out-of-phase χ'' component of GdCu₂ 33 nm measured at $f=0.2$ Hz. Note the χ'' units are expressed in μ emu/g·Oe. Memory effects are evidenced by the drop in the $\chi''_{warming} - \chi''_{cooling}$ curve below $T_{ag} = 15$ K. This drop is displayed in the bottom inset, which also includes the difference corresponding to 24-, 13- and 9-nm-sized MNPs. The $\chi''_{warming} - \chi''_{cooling}$ is divided by the respective χ''_{T_w} for each nanoparticle size to compare the drop accounting for the memory

effects. The top inset displays the χ'' vs. t curves recorded at $T_{ag} = 30$ K. **b)** and **c)** display the cycling protocol results of 33-nm-sized and 9-nm-sized MNPs, respectively. The relaxation is measured with $f = 0.2$ Hz at $T_{ag} = 15$ K before and after the temperature cycling. It can be seen that the SG state is completely reborn when the rise is of $T_{ag} + \Delta T = 1.06T_g$ in both MNP ensembles. Inset in **c)** compares the relaxation measured at $T_{ag} = 12, 15$ and 18 K for the 9-nm-sized MNPs

et al. 1998; Binder and Young 1984; Jonsson et al. 1995; Mydosh 2014). Figure 2a depicts the temperature dependence of out-of-phase component, measured while cooling down and letting the system stay at $T_{ag} = 15$ and 30 K for $t > 10^3$ s; and upon warming without making any stop. The inspection of the $\chi''_{warming} - \chi''_{cooling}$ difference showcased at the bottom inset allows to clearly detect memory effects below $T < 15$ K, as a drop in the difference is observable at temperatures below $T_{ag} = 0.83 T_g = 18$ K. This effect, which is triggered by the out-of-equilibrium dynamics ascribed to the freezing transition, shows up for all MNPs except for the 53- and 43-nm-sized ones. The lack of memory effects at the larger MNPs reveals that the AF-coupled core is still robust towards the magnetically frustrated surface phase. By comparing the drop in the $\chi''_{warming} - \chi''_{cooling}$ difference, two dif-

ferent trends can be deduced: (i) for the SAF MNPs (33 and 24 nm), the size reduction seems to reduce the memory effects, as the $\chi''_{warming} - \chi''_{cooling}$ difference is broader for the 18 nm ensemble as compared to the 33-nm-sized one. This is congruent with the stated more robust SG phase of the 33-nm-sized MNPs (Jefremovas et al. 2020b), as the RKKY exchange interactions are less affected by the micro-strain. Then, once the AF order is destroyed, and a SSG state is settled, (ii) memory effects get more intense as the nanoparticle size is reduced. Accordingly, the SSG MNPs (9-nm-sized) display stronger memory effects than those showcased by the 13-nm-sized ones. Both SSG ensembles display stronger memory effects compared to the SAF ensembles. This can be deduced from the sharpness of the $\chi''_{warming} - \chi''_{cooling}$ drop. Moreover, the inspection of

the top-right inset in Fig. 2a evidences the lack of a clear time-dependence associated to the high temperature dissipation (compare with Fig. 2b and c, where the time-dependence obeys the expected decay for spin glasses at several $T_{ag} < T_g$). This backs up the idea of a non-frustrated disordered phase, which is congruent with uncompensated AF moments, as it has been explained in the previous section.

In order to test the robustness of the SG phase, temperature cycling have been performed. To this aim, the MNPs were aged for $t \sim 10^3$ s at $T_{ag} = 15$ K. Then, the temperature was rose to $T_{ag} + \Delta T \approx 0.88, 0.97$ and $1.06 T_g$ and cycled back to T_{ag} . Immediately, the magnetization was recorded for $t \sim 10^4$ s. Figure 2b and c show results for these measurements performed in 33 nm (SAF) and 9 nm (SSG) sized MNPs, respectively. As it can be seen, both MNP ensembles achieve a completely reborn SG landscape (*rejuvenation*) when the cycling step is performed above T_g ($T + \Delta T \geq 1.06T_g$), as the χ'' post-cycle ($t > 10^3$ s) is equal to the former χ'' pre-cycle ($t = 0$ s). Also, in both MNP ensembles, the smaller the ΔT , the slower the relaxation towards equilibrium, which indicates that larger free-energy barriers are built. This reveals that the *domains* of correlated spins are larger (Jonason et al. 1998).

If we stick close to the *rejuvenation limit* by paying attention to the cycle performed at $T + \Delta T = 0.97T_g$, it can be observed how, despite the different global states (SAF and SSG), the SG freezing dynamics corresponding to 33- and 9-nm-sized MNPs behave in a very similar fashion. In this way, the $\chi''/\chi''(t=0)$ value at both 33 nm and 9 nm MNPs after the temperature cycle is around $\chi''/\chi''(t=0) = 0.98$, whereas it is already $\chi''/\chi''(t=0) = 1$ (fully recovered) for 24- and 13-nm-sized ones (not shown). This implies that the domains built for the former (33 and 9 nm) are larger, as the particular SG configuration is not completely *reborn* after the cycling. The reason beneath this feature further supports the static picture, from which it was deduced that the most interacting SG phase is settled for 33-nm-sized MNPs (Jefremovas et al. 2020b). Once the SSG state is established, the smaller the MNPs, the more robust the frustrated interactions among the spins.

Specific heat measurements

Specific heat analyses have been carried out separating the contributions stemming from the core and

the surface, following the same procedure as the one published in Jefremovas et al. (2021, 2022). To this aim, the experimental specific heat c_p is assumed to be the result of the lattice contribution $c_{lattice}$ (formed by the addition of the electronic and the phononic ones, i.e., $c_{el} + c_{ph}$), plus the magnetic c_{mag} . In the case of GdCu₂, since Gd³⁺ are S-state ions, no crystalline electric field (CEF) contribution is present in the GdCu₂ specific heat. Each core and surface contributions are weighted by the geometrical core and surface-to-volume ratios, respectively, which have been estimated in the same way as in precedent works (Jefremovas et al. 2021, 2022). Accordingly, the core and surface contributions are $N_c = 2.0$ (33 nm), 1.0 (13 nm) and 0.9 (9 nm), and $N_s = 3 - N_c$, respectively, as the number of atoms is $N = 3$). Therefore, the specific heat is modeled following:

$$c_{lattice} = N_c \left[\gamma_c \cdot T + 9R \left(\frac{T}{\theta_D^c} \right) \int_0^{\theta_D^c/T} dx \frac{x^4 \cdot e^x}{(e^x - 1)^2} \right] + N_s \left[\gamma_s \cdot T + 9R \left(\frac{T}{\theta_D^s} \right) \int_0^{\theta_D^s/T} dx \frac{x^4 \cdot e^x}{(e^x - 1)^2} \right] \quad (1)$$

Following this procedure, the green line in Fig. 3a represents the obtained $c_{lattice}$ for 33-nm-sized MNPs. Values of $\gamma^c = 6.7$ (2) mJ (molK²)⁻¹ and $\theta_D^c = 277$ (3) K have been obtained for this particular size, which agree well with the ones obtained for bulk alloy (not shown), and reported for polycrystalline bulk GdCu₂ (Podgornykh and Kourov 2007). The obtained γ^s and θ_D^s values for all the MNP sizes are listed in Table 1. There, it can be seen that both parameters increase with the size reduction, a fact that can be understood according to the increasing surface disorder and surface-to-core ratio.

The inset of this figure shows the magnetic entropy S_{mag} against the temperature. This S_{mag} has been obtained according to:

$$S_{mag}^{exp} = \int_0^{300} \frac{c_{mag}}{T} dT \quad (2)$$

The experimental magnetic entropy (18 J/mol·K) and the calculated $S_{mag}^{theo}(300K) = R[\ln(2J + 1)] = 17.29$ J/mol·K are in good agreement. The value of S_{mag}^{exp} is already ≈ 18 J/mol·K at $T = 100$ K. This indicates that the energy levels are fully populated at a lower temperature than expected. This trend, which holds for all the GdCu₂ MNPs, may be indicative of the existence of quadrupolar and/or higher order interactions (Luong and Franse 1995; Morin and Schmitt 1990).

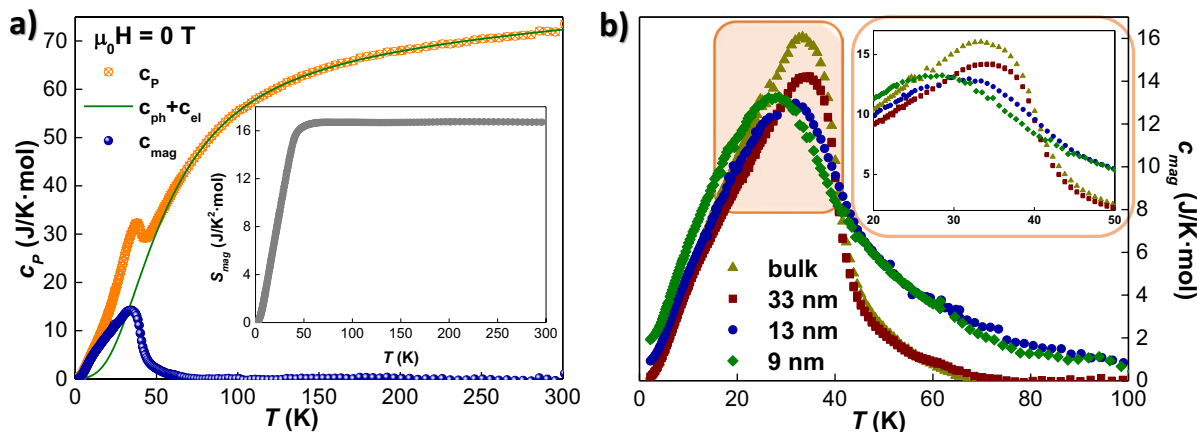


Fig. 3 **a)** Measured specific heat (orange) together with the c_{latice} (green) and the c_{mag} contributions for GdCu₂ 33 nm MNPs. The inset includes the magnetic entropy corresponding to this MNP size, where it can be seen that saturation is almost

achieved around $T_N=40$ K. **b)** c_{mag} contribution corresponding to bulk, 33-, 13- and 9-nm-sized MNPs. Inset zooms the region surrounding the hump contribution to c_{mag} . All the measurements have been performed under no external applied field

Table 1 Values for surface Sommerfeld coefficient γ^s , Debye Temperature, θ_D^s , and N_c ratio, for GdCu₂ 33-, 13- and 9-nm-sized MNP ensembles, obtained according to Eq. 1

$\langle D \rangle$ (nm)	γ^s (mJ mol ⁻¹ K ⁻²)	θ_D^s (K)	N_c
33	15.8(1)	144(1)	2.0
13	26.1(6)	238(1)	1
9	33.9(1)	265(2)	0.9

Figure 3b depicts the c_{mag} vs. T dependency for bulk, 33-, 13- and 9-nm-sized MNPs. It is worth noting the two sources of c_{mag} evidenced by the bulk and 33-nm-sized alloys. Accordingly, the AF-coupled magnetic moments give rise to a λ -like peak anomaly, located at $T \sim 40$ K. This contribution should show a slight left-shift with the size reduction, owing to the reduction of the amount of AF-coupled moments (García-Saiz et al. 2014; Chevalier et al. 2006). Nevertheless, no shift is found in our GdCu₂ alloys, as it was also the case of the $M_{DC}(T)$ curves shown by Jefremovas et al. in (2020b). This underlines, in agreement with the dynamic $\chi_{AC}(t,f,T)$ characterization, the robustness of the AF order. Additionally to the AF λ -anomaly, at temperatures below T_N , a broad hump, which can be ascribed to a Schottky-like contribution (Gopal 2012), emerges for these bulk and 33-nm-sized MNPs. In the present case of GdCu₂, the occurrence of this Schottky contribution should

be ascribed to the Zeeman splitting of the eightfold degenerate energy level, rather than to CEF effects (as Gd³⁺ is $L = 0$) or spin wave propagation (Luong and Franse 1995; Luong et al. 1985). Furthermore, the fact that the excess of c_{mag} drops to zero for $T > T_N$ rules out the possibility of a CEF-motivated contribution to c_p (Gopal 2012), and it is congruent with the results reported for GdCu₂ single-crystal (Koyanagi et al. 1998) and for GdCu_x bulk antiferromagnets (Podgornykh and Kourov 2007). Both contributions (AF λ -anomaly and Schottky contributions) are so close to each other that they overlap, resulting in a single broad cusp, rather than in two separated signatures.

On the other hand, the $c_{\text{mag}}(T)$ dependency of the SSG 13- and 9-nm-sized MNPs evidences a broad cusp at $T \sim 31$ (13 nm) and $T \sim 27$ K (9 nm), with a tail (asymptotic decrease to zero of the c_{mag}) that extends up to $T \sim 100$ K. The cusp intensity is reduced with respect to the one of bulk and 33 nm MNPs, and it is also found at lower temperatures. The interpretation of the c_{mag} of these SSG MNPs is very alike to the one already commented for bulk and 33-nm-sized MNPs. Even though the AF interactions are not strong enough to give rise to a collective well-defined ordered state within these SSG MNPs, they still exist within the sample, as they are a basic requirement for magnetic frustration (Mydosh 2014). Consequently, it could be possible that some regions

of the MNPs give rise to an *effective* local field, which splits the multiplets (Zeeman splitting), resulting in a contribution to c_{mag} . Of course, as the AF order interactions are further diminished by reducing the MNP size (increasing disorder), this splitting gets smaller, thus, the hump shifts towards lower temperature value. Finally, the c_{mag} asymptotically decreases to zero, a fact that contrasts with the drop observed for bulk and 33-nm-sized MNPs. This tail shall be ascribed to the SG-frustrated moments, which may give rise to (tiny) contributions to the specific heat at higher temperatures (Martin 1979; Mydosh 2014; Gopal 2012; Arons et al. 1994).

Conclusions

The dual magnetic disorder dynamics in ensembles of GdCu₂ magnetic nanoparticles (53- to 7-nm-sized) has been unraveled. On the one hand, at low temperature ($T_g \lesssim 18$ K), an interacting SG phase is well-established, evidencing rejuvenation and memory effect phenomena. This frustrated phase comes as a result of the size reduction to the nanoscale, driven by (i) the surface frustrated moments for the case of SAF nanoparticles (53-, 43-, 33- and 24-nm-sized), and (ii) the whole nanoparticle, for the case of SSG-ones (13 and 9 nm). On the other hand, a high temperature ($T_{d1} \sim 33$ K and $T_{d2} \sim 40$ K) non-frustrated disordered phase has been found only for the SAF nanoparticles. This dissipation, which does not evidence a time dependency of the AC susceptibility, and therefore magnetic ageing, is not present for the SSG nanoparticles. This necessarily connects the high-temperature dissipation to a disorder driven by the uncompensated AF moments, found at the AF grain boundaries. The observation of two cusps for this high-temperature disorder is intimately related to the cycloidal propagation of the GdCu₂ magnetic structure, which includes left and right-handed domains. Our results demonstrate the importance of ageing and specific heat as powerful tools to unravel the subtleties concerning the spin dynamics in magnetic GdCu₂ nanoparticles.

Funding Open Access funding provided thanks to the CRUE-CSIC agreement with Springer Nature. This work has been financially supported by Spanish MCIU MAT2017–83631–C3–R project. EMJ work was supported by ‘Beca Concepción Arenal’ BDNS: 406333 (Gobierno de Cantabria–Universidad de Cantabria).

Data availability The raw/processed data required to reproduce these findings cannot be shared at this time due to technical or time limitations.

Declarations

Conflict of interest The authors declare no competing interests.

Open Access This article is licensed under a Creative Commons Attribution 4.0 International License, which permits use, sharing, adaptation, distribution and reproduction in any medium or format, as long as you give appropriate credit to the original author(s) and the source, provide a link to the Creative Commons licence, and indicate if changes were made. The images or other third party material in this article are included in the article’s Creative Commons licence, unless indicated otherwise in a credit line to the material. If material is not included in the article’s Creative Commons licence and your intended use is not permitted by statutory regulation or exceeds the permitted use, you will need to obtain permission directly from the copyright holder. To view a copy of this licence, visit <http://creativecommons.org/licenses/by/4.0/>.

References

- Arons R, Loewenhaupt M, Reif T, Gratz E (1994) The magnetic structures of NdCu₂ in zero field. *J Phys Condens Matter* 6(34):6789
- Bachmann R, DiSalvo FJr, Geballe T, Greene R, Howard R, King C, Kirsch H, Lee K, Schwall R, Thomas H-U et al (1972) Heat capacity measurements on small samples at low temperatures. *Rev Sci Instrum* 43(2):205–214
- Baczewski L, Piecuch M, Durand J, Marchal G, Delcroix P (1989) Influence of interface effects on a rare-earth crystal field in iron–rare-earth multilayers. *Phys Rev B* 40(16):11237
- Binder K, Young A (1984) Logarithmic dynamic scaling in spin-glasses. *Phys Rev B* 29(5):2864
- Chevalier B, Matar SF, Ménétrier M, Marcos JS, Fernández JR (2006) Influence of Ce–H bonding on the physical properties of the hydrides CeCoSiH_{1.0} and CeCoGeH_{1.0}. *J Phys Condens Matter* 18(26):6045
- Coey JM (2010) *Magnetism and magnetic materials*. Cambridge university press
- Döbrich F, Elmas M, Ferdinand A, Markmann J, Sharp M, Ecklerle H, Kohlbrecher J, Birringer R, Michels A (2009) Grain-boundary-induced spin disorder in nanocrystalline gadolinium. *J Phys: Condens Matter* 21(15):156003
- Everschor-Sitte K, Masell J, Reeve RM, Kläui M (2018) Perspective: Magnetic skyrmions—overview of recent progress in an active research field. *J Appl Phys* 124(24):240901
- Fukami S, Lorenz VO, Gomonay O (2020) Antiferromagnetic spintronics. *J Appl Phys* 128(7):070401. AIP Publishing LLC
- García-Saiz A, de Pedro I, Migowski P, Vallcorba O, Junquera J, Blanco JA, Fabelo O, Sheptyakov D, Waerenborgh

- JC, Fernandez-Díaz MT et al (2014) Anion- π and halide-Halide nonbonding interactions in a new ionic liquid based on imidazolium cation with three-dimensional magnetic ordering in the solid state. *Inorganic Chem* 53(16):8384–8396
- Golosovsky I, Mukhin A, Skumryev V, Boehm M, Schmidt W, Regnault L-P, Gudim I (2021) Magnetic excitations and exchange interactions in the substituted multiferroics (nd, tb) fe 3 (bo 3) 4 revealed by inelastic neutron scattering. *Phys Rev B* 103(21):214412
- Gopal E (2012) Specific heats at low temperatures. Springer Science & Business Media
- Greedan JE (2006) Frustrated rare earth: magnetism Spin glasses, spin liquids and spin ices in pyrochlore oxides. *J Alloys Compd* 408:444–455
- Guinier A (1994) X-ray diffraction in crystals, imperfect crystals, and amorphous bodies. Courier Corporation
- Gyax F, Andreica D, Schenck A, Ōnuki Y (2002) Probing the magnetic structure of GdCu₂ by μ sr spectroscopy. *J Magn Mater* 246(1–2):101–109
- Jefremovas EM et al (2020a) Exploring the different degrees of magnetic disorder in Tb_xR_{1-x}Cu₂ nanoparticle alloys. *Nanomaterials* 10(11):2148
- Jefremovas E, Alonso J, De la Fuente Rodríguez M, Fernández JR, Espeso J, Rojas D, García-Prieto A, Fernández-Gubieda M, Barquín LF (2020b) Investigating the size and micro-strain influence in the magnetic order/disorder state of GdCu₂ nanoparticles. *Nanomaterials* 10(6)
- Jefremovas E, de la Fuente Rodríguez M, Damay F, Fåk B, Michels A, Blanco JA, Barquín LF (2021) Observation of surface magnons and crystalline electric field shifts in superantiferromagnetic NdCu₂ nanoparticles. *Phys Rev B* 104:134404
- Jefremovas E, Svedlindh P, Damay F, Alba Venero D, Michels A, Blanco JA, Barquín LF (2022) Magnetic order and disorder environments in NdCu₂ nanoparticles. *Sci Rep* 12:9733. <https://doi.org/10.1038/s41598-022-13817-7>
- Jonason K, Vincent E, Hammann J, Bouchaud J, Nordblad P (1998) Memory and chaos effects in spin glasses. *Phys Rev Lett* 81(15):3243
- Jönsson P, Hansen MF, Svedlindh P, Nordblad P (2000) Memory effects in an interacting magnetic nano-particle sample. *Phys B Condens Matter* 284:1754–1755
- Jonsson T, Mattsson J, Djurberg C, Khan F, Nordblad P, Svedlindh P (1995) Aging in a magnetic particle system. *Phys Rev Lett* 75(22):4138
- Joshi D, Gebresenbut G, Gomez CP, Mathieu R (2020) Memory and rejuvenation in a quasicrystal. *EPL (Europhysics Lett)* 132(2):27002
- Jungfleisch MB, Zhang W, Hoffmann A (2018) Perspectives of antiferromagnetic spintronics. *Phys Lett A* 382(13):865–871
- Jungwirth T, Marti X, Wadley P, Wunderlich J (2016) Antiferromagnetic spintronics. *Nat Nanotechnol* 11(3):231–241
- Koyanagi A, Yoshida Y, Kimura Y, Settai R, Sugiyama K, Ōnuki Y (1998) Magnetic and electrical properties of GdCu₂. *J Phys Soc Jpn* 67(7):2510–2513
- Lebrun R, Ross A, Bender S, Qaiumzadeh A, Baldrati L, Cramer J, Brataas A, Duine R, Kläui M (2018) Tunable long-distance spin transport in a crystalline antiferromagnetic iron oxide. *Nature* 561(7722):222–225
- Luong H, Franse JJM (1995) Magnetic properties of rare earth-Cu₂ compounds, 8th edn. Elsevier Science B.V., pp 415–488
- Luong NH, Franse J, Hien TD (1985) Specific heat and thermal expansion in GdxY1-xCu2. *J Phys F: Metal Phys* 15(8):1751
- Marti X, Fina I, Frontera C, Liu J, Wadley P, He Q, Paull R, Clarkson J, Kudrnovský J, Turek I et al (2014) Room-temperature antiferromagnetic memory resistor. *Nat Mater* 13(4):367–374
- Martin DL (1979) Specific heat of spin-glass cuMn below 3 K. *Phys Rev B* 20(1):368
- Morin P, Schmitt D (1990) Quadrupolar interactions and magneto-elastic effects in rare earth intermetallic compounds. *Handb Ferromagn Mater* 5:1–132
- Mydosh JA (2014) Spin glasses: an experimental introduction. CRC Press
- Nakatsuji S, Kiyohara N, Higo T (2015) Large anomalous hall effect in a non-collinear antiferromagnet at room temperature. *Nature* 527(7577):212–215
- Nordblad P, Svedlindh P (1998) Experiments on spin glasses. *Spin Glasses and Random Fields*, World Scientific, 1–27
- Park H-K, Kim S-K (2021) Channeling of spin waves in antiferromagnetic domain walls. *Phys Rev B* 103(21):214420
- Podgornykh S, Kourov N (2007) Low-temperature specific heat of gdcu, gdcu2, and gdcu5 antiferromagnets. *Bull Russ Acad Sci Phys* 71(8):1079–1080
- Rojas D, Barquín LF, Fernández JR, Espeso J, Sal JG (2007) Size effects in the magnetic behaviour of TbAl₂ milled alloys. *J Phys: Condensed Matter* 19(18):186214
- Rotter M, Lindbaum A, Gratz E, Hilscher G, Sassik H, Fischer H, Fernandez-Diaz M, Arons R, Seidl E (2000) The magnetic structure of GdCu₂. *J Magn Magn Mater* 214(3):281–290
- Rotter M, Lindbaum A, Gratz E, Hilscher G, Sassik H, Fischer H, Fernández-Diaz M, Arons R, Seidl E (2000) The magnetic structure of GdCu₂. *J Magn Magn Mater* 214(2000):281–290
- Rotter M, Schneidewind A, Loewenhaupt M, Doerr M, Stunault A, Hiess A, Lindbaum A, Gratz E, Hilscher G, Sassik H (2000) Magnetic scattering on GdCu₂. *Phys B Condens Matter* 284:1329–1330
- Rotter M, Schneidewind A, Loewenhaupt M, Doerr M, Stunault A, Hiess A, Lindbaum A, Gratz E, Hilscher G, Sassik H (2000) Magnetic scattering on GdCu₂. *Phys B Condens Matter* 284:1329–1330
- Svedlindh P, Gunnarsson K, Andersson J-O, Katori HA, Ito A (1992) Time-dependent ac susceptibility in spin glasses. *Phys Rev B* 46(21):13867
- Takano K, Kodama R, Berkowitz A, Cao W, Thomas G (1997) Interfacial uncompensated antiferromagnetic spins: Role in unidirectional anisotropy in polycrystalline Ni81Fe19/CoO bilayers. *Phys Rev Lett* 79(6):1130
- Tokura Y, Kanazawa N (2020) Magnetic skyrmion materials. *Chem Rev* 121(5):2857–2897
- von Malottki S, Dupé B, Bessarab PF, Delin A, Heinze S (2017) Enhanced skyrmion stability due to exchange frustration. *Sci Rep* 7(1):1–10
- Welch PG, Paddison JA, Le MD, Gardner JS, Chen W-T, Wildes AR, Goodwin AL, Stewart JR (2022) Magnetic structure and exchange interactions in the heisenberg pyrochlore antiferromagnet Gd₂Pt₂O₇. *Phys Rev B* 105(9):094402

- Yuan H, Gomonay O, Kläui M (2017) Skyrmions and multisublattice helical states in a frustrated chiral magnet. *Phys Rev B* 96(13):134415
- Zhang X, Zhou Y, Ezawa M (2016) Antiferromagnetic skyrmion: stability, creation and manipulation. *Sci Rep* 6(1):1–8
- Zhao L, Li C, Hao Z, Liu X, Liao X, Zhang J, Su K, Li L, Yu H, Greneche J-M et al (2019) Influences of element segregation on the magnetic properties in nanocrystalline nd-ce-fe-b alloys. *Mater Charact* 148:208–213
- Zvyagin A (2013) New physics in frustrated magnets: Spin ices, monopoles, etc. *Low Temp Phys* 39(11):901–922

Publisher's note Springer Nature remains neutral with regard to jurisdictional claims in published maps and institutional affiliations.